Ocean Engineering 305 (2024) 117975

Contents lists available at ScienceDirect

Ocean Engineering

journal homepage: www.elsevier.com/locate/oceaneng

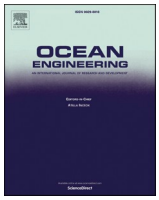

Research paper

Design and optimisation of a 20 MW offshore wind turbine blade

Pavana Koragappa, Patrick G. Verdin *

Energy & Sustainability, Cranfield University, Cranfield, Bedfordshire, MK43 0AL, UK

ARTICLE INFO

Keywords:
Offshore wind turbine
Blade length
Pitch
rpm
Optimisation

ABSTRACT

In the global pursuit of Net Zero emissions by 2050, wind turbines have become a leading solution. These renewable energy generators offer a trifecta of benefits, significantly reducing CO_2 emissions, minimizing environmental impact, and delivering cost-competitive clean power. However, the key to maximizing their potential lies in the aerodynamic design of the turbine blades. By improving the blade performance, researchers and engineers can significantly increase wind energy capture, propelling wind turbines to the forefront of the global transition to a sustainable future. Higher power generating wind turbines are needed to reach the Net Zero target. By upscaling the "DTU 10 MW Reference Wind Turbine", this research has achieved an aerodynamically stable 20 MW offshore wind turbine blade design. Variable rotation speed and variable pitch angle configurations have been considered to achieve an ideal power curve. The aerodynamic performance has been evaluated and quantified for a length optimised blade design, wherein the power and thrust have been increased by 80.84% and 88.67%, respectively, at a rated wind velocity of 12 m/s.

1. Introduction

For the last decades, research and development projects related to wind energy have intensified. Offshore wind turbines now form a key-part of the Energy mix to reach the Net-Zero target by 2050. However, it is also now crucial to consider improving existing wind turbines further and improve their design and efficiency at lower cost (Sørensen, 2011). Different solutions have been proposed to improve wind energy harvesting. Although a simple solution is to attach a winglet at the tip of the blades, the improvement would be minimal (Gasch and Twele, 2012). A second solution is to extend any wind farm by placing additional wind turbines of same efficiency to generate additional power (Vartan, 2021). A third option is to design a large-scale wind turbine which can produce a higher power (Jonkman et al., 2009). The latter option has been investigated in this work.

There are several important aspects to take into account when designing a large-scale wind turbine, mainly related to the structural (Kong et al., 2005) and aerodynamic performance (Schepers and Schreck, 2019; Wilson and.S, 1974; Hand et al., 2001). An efficient structural design would reduce the material and maintenance costs of the turbine, and would improve its aerodynamic efficiency, generating a higher amount of power (Vartan, 2021). The current research aims to produce a 20 MW horizontal axis wind turbine blade design, which is the highest power reached to date worldwide.

The conversion of kinetic energy into mechanical energy has been studied and improved for decades and maximizing the utilization of the kinetic energy of the wind was one of the objectives of this work. The Blade Element Momentum theory (BEMT) has been traditionally used to develop the rotor blades of wind turbines and assess their performance behaviour (Manwell et al., 2010). Many studies have been carried out on small scale horizontal axis wind turbines using BEMT, Computational Fluid Dynamics (CFD) and experimental methods (Jonkman et al., 2009; Manwell et al., 2010; Barlas and van Kuik, 2010). While commercial large-scale offshore wind turbines hold high promise for clean energy generation due to their ability to capture substantial wind power, further research and development (R&D) is essential to maximize their potential.

A wide range of studies have been performed on rotor blades aerofoils (Kong et al., 2005; Schepers and Schreck, 2019; Fuglsang and Bak, 2004; Bjorck, 1990). The higher the thickness the better the structural properties, but this also affects the blades' aerodynamic efficiency. Hence the blade thickness is limited to 21%–27% (Bak et al., 2013). Flygtekniska Forsoksanstalten Airfoils (FFA) (Bjorck, 1990) developed by the Aeronautical Research Institute of Sweden and Delft University (DU) are the preferred aerofoils because of the thickness and lift to drag ratio they can achieve (Wilson and.S, 1974).

Research on vortex reduction (or wake effect) and turbulence levels showed that designing and optimizing winglets do not contribute much to the power coefficient (Mourad et al., 2020; Maughmer, 2003; Gaunaa

* Corresponding author.
E-mail address: p.verdin@cranfield.ac.uk (P.G. Verdin).

https://doi.org/10.1016/j.oceaneng.2024.117975
Received 1 October 2023; Received in revised form 8 April 2024; Accepted 20 April 2024
Available online 24 April 2024

Nomenclature

Symbol	*Description*	*Unit*
A	Rotor swept area	m^2
C_P	Power coefficient	
C_T	Thrust coefficient	
E	Kinetic energy	Nm
EI	Bending stiffness	N/m^2
m	Mass	kg
$\dot{m}$	Mass flow rate	kg/s
M	Bending moment	Nm
P	Power	W
R	Rotor radius	m
r	Rotor radial station	m
sf	Scaling factor	
U	Wind velocity	m/s
ρ	Density	kg/m^3

Table 1
Properties for 5–20 MW wind turbine using simple scaling approach (Sieros et al., 2012).

Power (MW)	Blade diameter (m)	Hub height (m)	Tip speed (m/s)
5	126	90	80
10	178	116	80
15	218	136	80
20	252	153	80

Table 2
Basic key parameters of 10 and 20 MW wind turbines.

Key parameters of the wind turbines		
Parameters	DTU 10 MW RWT	20 MW WT
Rated power (*MW*)	10	20
Number of blades	3	3
Rotor placement	Upwind	Upwind
Rotor diameter (*m*)	178.3	252
Hub diameter (*m*)	5.6	8
Hub height (*m*)	119	167.9
Blade Length (*m*)	86.4	122
Rated wind speed (*m/s*)	11.4	12
Minimum rotor Speed (*rpm*)	6	4.4
Rated rotor speed (*rpm*)	9.6	9.2
Optimal TSR	7.5	9

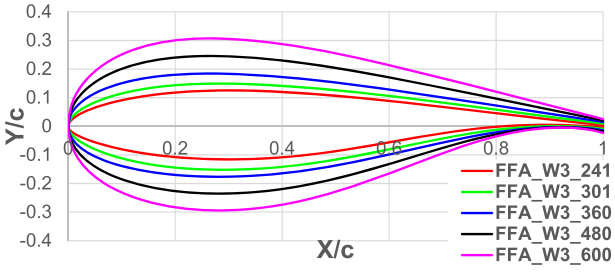

Fig. 1. FFA-W3 series aerofoils used for the 2D studies.

and Johansen, 2007a, 2007b; Farhan et al., 2019; Eppler, 1997). Varying the pitch and flap design (Shimizu and Kamada, 2001) for a large wind turbine makes the design complex and expensive, and manufacturers require a simple design for ease of fabrication. A "5 MW Reference Wind Turbine" was thus designed to overcome all these issues in 2009

Table 3
Upscaled wind turbine blade geometry parameters.

Aerofoils	Radial station r (m)	Radial station (r)/Rotor radius (R)	Chord (m)	Twist (°)	Thread Axis (%chord)
Cylinder	0	0	5.38	0	0.5
	3.91	0.03	5.38	14.5	0.5
FFA-W3-600	15.5	0.12	5.45	14.43	0.44
	23.81	0.19	5.87	12.54	0.4
FFA-W3-480	29.48	0.23	6.11	9.96	0.37
FFA-W3-360	36.67	0.29	6.2	7.83	0.35
	43.22	0.34	6.09	6.72	0.35
FFA-W3-301	51.28	0.41	5.79	5.62	0.35
FFA-W3-241	71.19	0.57	4.7	2.89	0.35
	84.92	0.67	3.87	0.9	0.35
	101.93	0.81	2.9	−1.14	0.35
	119.95	0.95	1.9	−2.95	0.35
	126	1	0.6	−3.43	0.35

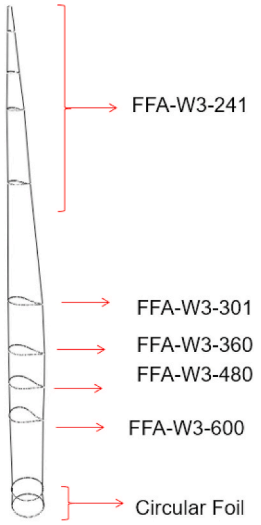

Fig. 2. 3D blade geometry for upscaled blade.

(Hand et al., 2001). Later, in 2011 (Frøyd and Dahlhaug, 2011) and 2013 (Bak et al., 2014), a "10 MW Reference Wind Turbine" was designed, where the classical similarity rules were used to upscale the rotor blades. In the present research, a better performing large scale offshore wind turbine has been designed through varying critical aerodynamic parameters using CFD.

Quick results can be generated using any software based on the Blade Element Momentum (BEM) theory. One example is QBlade, which is an open-source tool designed to calculate wind turbine aerodynamics. Tools such as FAST, TurboSim and AeroDyn have also been previously used to generate wind turbine blade models (Ashuri et al., 2016). They are similar to QBlade and are based on the BEM theory to obtain the power curve.

Power output and aerodynamic loads can be obtained through the aerodynamics of a wind turbine. Various degrees of complexity and accuracy of a wind turbine model can be determined by those aerodynamics loads (Thé and Yu, 2017). Using the BEM methodology, two-dimensional (2D) data of an aerofoil can be generated for the design phase (Sørensen, 2011). To reduce the computational cost, the flow physics can be studied through three dimensional (3D) inviscid vortex approaches. Navier-Stokes equations are neglected when considering the results of the two above-mentioned approaches. CFD can then used to resolve the next stage of the model development.

QBlade has been used in this work as a basic design point, and to

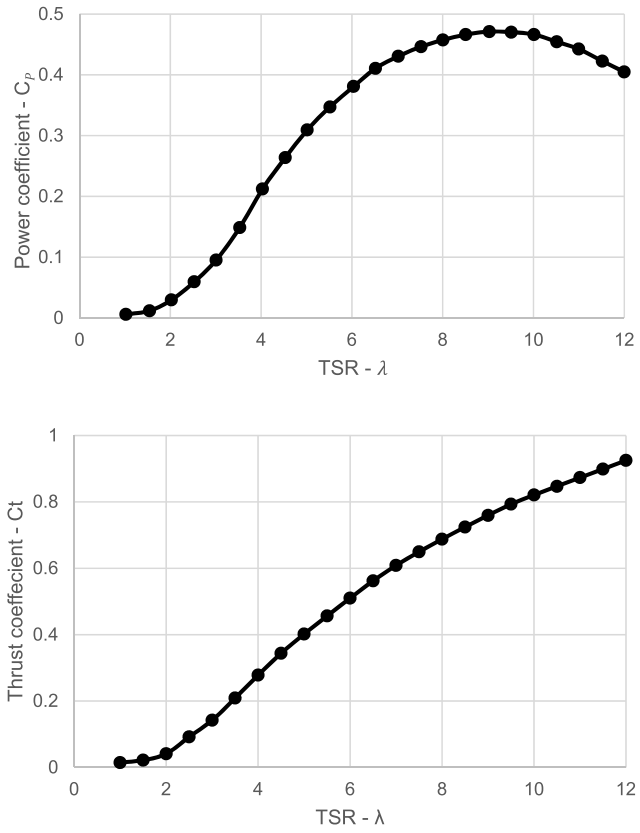

Fig. 3. Power coefficient Cp and Thrust coefficient Ct vs tip speed ratio for an upscaled blade.

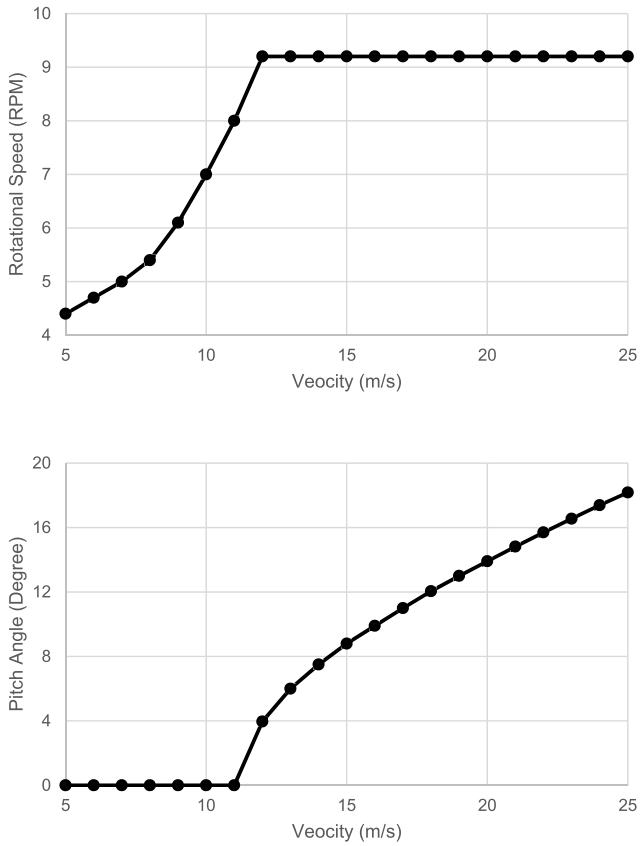

Fig. 4. Aerodynamic performance parameters vs Velocity.

Table 4
Operational parameters and aerodynamic results at different velocities (the * symbols indicate the velocities to be simulated in CFD).

Velocity (m/s)	Rotational speed (RPM)	Pitch angle (degree)	Power (MW)	C_P	Thrust (MN)	C_t
5*	4.4	0.00	1.59	0.416	0.690	0.903
6*	4.7	0.00	2.90	0.439	0.989	0.899
7*	5.0	0.00	4.80	0.458	1.170	0.782
8*	5.4	0.00	7.29	0.466	1.520	0.777
9*	6.1	0.00	10.40	0.467	1.920	0.776
10*	7.0	0.00	14.27	0.467	2.390	0.782
11*	8.0	0.00	19.00	0.467	2.920	0.790
12*	9.2	3.96	20.20	0.383	2.500	0.568
13*	9.2	6.00	20.20	0.301	2.200	0.426
14*	9.2	7.50	20.20	0.241	1.980	0.331
15*	9.2	8.80	20.20	0.196	1.800	0.262
16*	9.2	9.90	20.20	0.161	1.695	0.217
17*	9.2	11.00	20.20	0.135	1.600	0.181
18*	9.2	12.05	20.20	0.113	1.510	0.153
19*	9.2	13.00	20.20	0.096	1.480	0.134
20*	9.2	13.91	20.20	0.083	1.405	0.115
21*	9.2	14.82	20.20	0.071	1.390	0.103
22*	9.2	15.70	20.20	0.062	1.320	0.089
23*	9.2	16.55	20.20	0.054	1.290	0.080
24*	9.2	17.39	20.20	0.048	1.260	0.072
25*	9.2	18.18	20.20	0.042	1.240	0.065

check the power generation from the new proposed designs. Although results can be generated quickly, BEM-based tools are not fully accurate since viscous effects are not accounted for. When considering CFD, the fluid flow is described through the Navier-Stokes equations which are derived for the conservation of momentum which, when merged with the continuity equation, can determine the flow physics of a Newtonian fluid and an incompressible flow in three dimensions (Versteeg and Malalasekera, 2012). From the conservation law of energy, an equation for compressible flow can be derived by including the density. Unlike simpler methods, CFD offers a high-resolution view of the aerodynamic forces acting across different sections of the blade. This detailed analysis makes CFD ideal for optimizing blade shapes, investigating complex airflow patterns, and conducting in-depth wind turbine design analysis.

An investigation on the pre-design process for a 20 MW wind turbine and its control system was performed previously (Peeringa et al., 2011). The approach involved initially scaling up a proven 5 MW Upwind design (Van Langen and Hendrinks, 2010). Subsequently, the authors used the design tools WMC/ECN within the Focus6 suite, to perform the structural analysis and the control design of the turbine blades in a sequential manner. Once the blade design was finalized, a control system was developed to complement the finalized turbine configuration (Peeringa et al., 2011). A 20 MW common research model was developed using a Multidisciplinary design optimisation approach, which is a well-known approach for wind turbine design, by upscaling the 5 MW Upwind (Van Langen and Hendrinks, 2010). They finally defined the Aeroservoelastic design to make it publicly available for further research (Ashuri et al., 2016). In the current research, the method is slightly different as the upscaling was carried out from the “DTU 10 MW RWT” (Bak et al., 2014) using classical similarity rules, and the model was aerodynamically optimised using CFD.

2. Upscaling of wind turbines

Across Europe, 5–6 MW wind turbines have been widely installed offshore, generating up to 500 MW power in a wind farm (Wilson, 2020). The ‘Up Wind Research Project’ (Sørensen, 2011) supported by EU further considered the challenges that may arise to design a higher power generating wind turbine. For instance, a 20 MW wind turbine would require a very large rotor with an approximate diameter of 250 m

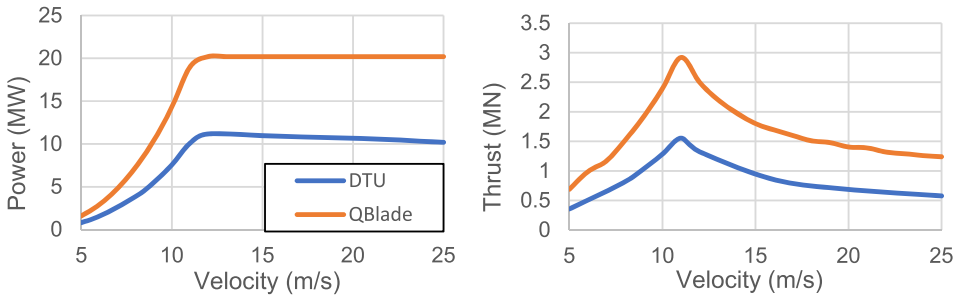

Fig. 5. Power and thrust versus velocity plot – DTU 10 MW wind turbine and this work 20 MW wind turbine.

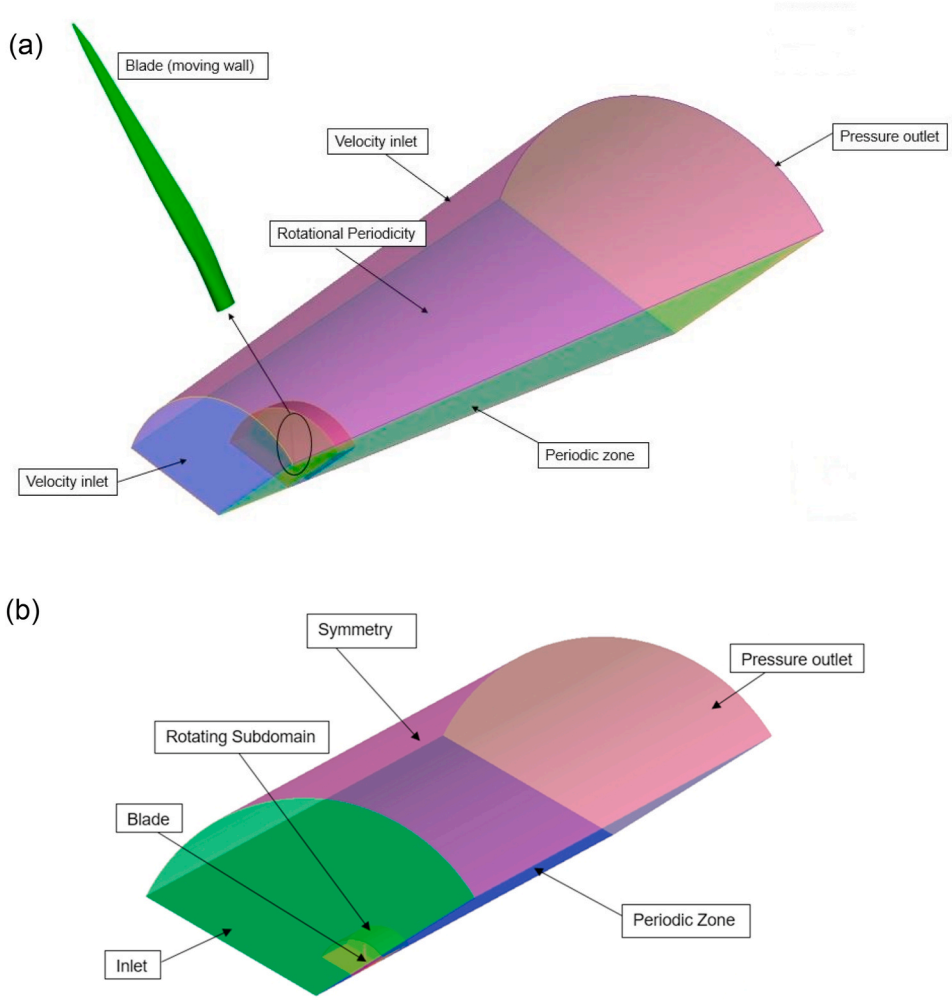

Fig. 6. Conical (a) and cylindrical (b) shaped domains.

and a tower height exceeding 150 m (Sørensen, 2011). These large wind turbines will give rise to weight and load issues (Bossanyi, 2003) which are not desired and will need intense attention and further investigation in the design phase. Future trends, however, envision the need for high power generating wind turbines, producing at least 20 MW, to be able to obtain an annual energy production of 105 GWh (Gasch and Twele, 2012).

A common starting point for designing large wind turbines is based on geometric similarity scaling. This approach assumes that the turbine shape and aerodynamic behavior (including maintaining a constant tip speed) remain proportional as the size increases (Sieros et al., 2012). This method offers a preliminary assessment of critical aspects, including operation and structural integrity. It also highlights potential challenges that might arise during upscaling (Chaviaropoulos, 2007).

When geometric similarity is applied, the weight (m) and power (P) of the turbine scale with the cube (sf^3) and square (sf^2) of a scaling factor (sf), respectively. Aerodynamic forces follow a square relationship (sf^2) with the scaling factor, due to the increase in area. However, the moments generated by these forces scale as a cube (sf^3). Interestingly, the section bending stiffness (EI) exhibits an even faster scaling rate, following a power of four (sf^4). This characteristic leads to bending stresses from aerodynamic forces remaining constant relative to the size

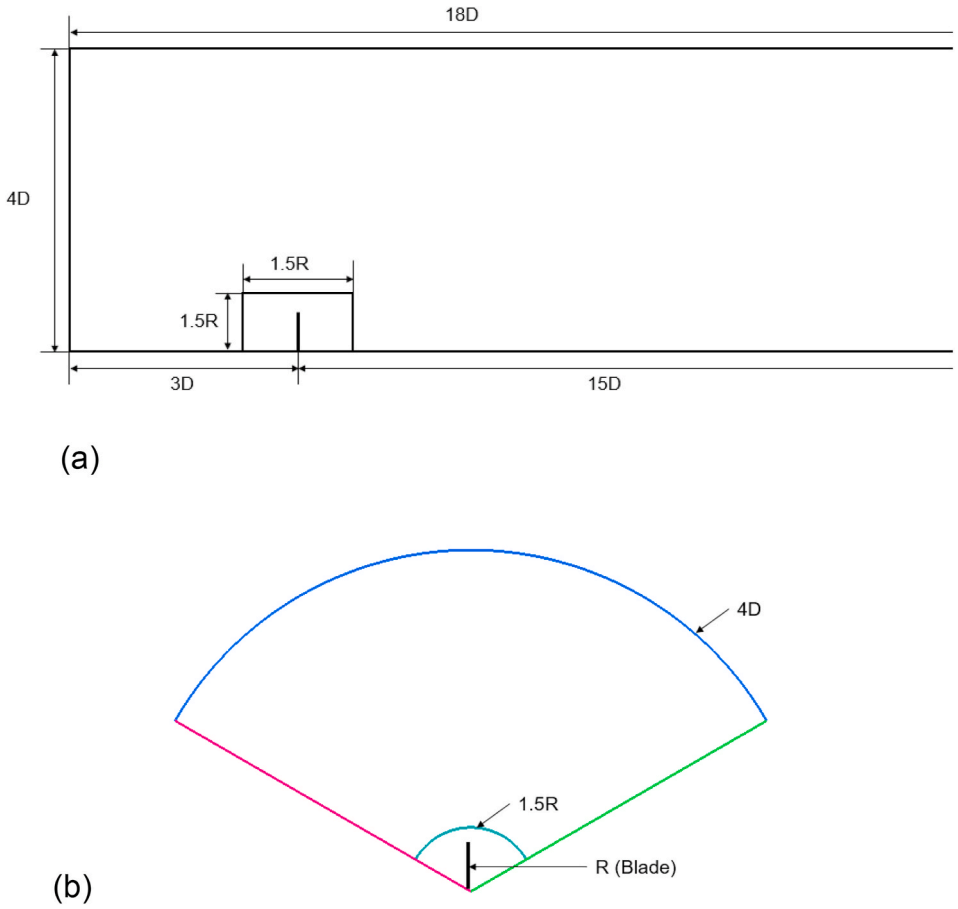

Fig. 7. Dimensions of the CFD domain: side view (a), front view (b), D-diameter, and R-radius of the blade.

Table 5
Boundary condition interaction and placement sensitivity.

Boundary Cond.	Cases	Selected
Domain shape	Conical and Cylindrical	Cylindrical
Number of blades	1 blade, 3 blades	1 blade
Inlet boundary (velocity inlet)	3D and 6D upstream	3D upstream
Outer domain (symmetry)	4D, 7.5D, and 12D	4D
Outlet boundary (pressure outlet)	7D, 10D, 15D 20D downstream	15D downstream
Subdomain	1.5R and 2.5R	1.5R
Time	Steady and Transient	Steady
Models	SA, k-ε (standard and realizable), k-ω SST, transition k-kl-ω, and DES	k-ω SST
Rotating domain	outer and subdomain, subdomain only	Subdomain only

increase ($M * y = EI$, with M the bending moment and y the radius of curvature).

A similar principle applies to tension stresses. Centrifugal forces scale with a combination of the turbine mass (m), angular velocity (ω), and blade radius (R). As the tip speed remains constant, the overall tension force increases with the square of the scaling factor (sf^2). The cross-section also scales with (sf^2), resulting in unchanging tension stresses. In contrast, the tension/compression and bending loads caused by the turbine's own weight, scale with (sf^3) and (sf^4), respectively. This translates to a proportional increase in the corresponding stresses as the turbine gets bigger.

Current research is moving towards incorporating more intricate aerodynamic effects while maintaining the assumption of linear structural behavior. This approach forms the basis for what is known as "classical similarity laws" (Chaviaropoulos, 2007). A key finding from these laws is that stresses due to aerodynamic forces experience minimal change during upscaling. However, stresses due to the turbine's own weight increase proportionally with the turbine size increase.

Table 6
Turbulence models and time setting cases for 25 m/s.

	CFD	DTU	CFD	DTU	Error [%]		
Model	C_t	C_t	C_P	C_P	C_t	C_P	Time
SA	0.017	0.06	0.003	0.043	−72.22	−93.52	Steady
k-ε (standard)	0.024	0.06	0.006	0.043	−59.66	−84.91	Steady
k-ε (realizable)	0.031	0.06	0.017	0.043	−48.55	−61.08	Steady
k-ω SST	0.059	0.06	0.043	0.043	−0.993	−0.087	Steady
transition k-kl-ω	0.032	0.06	0.019	0.043	−46.33	−56.45	Steady
DES	0.044	0.06	0.026	0.043	−26.67	−39.54	Transient

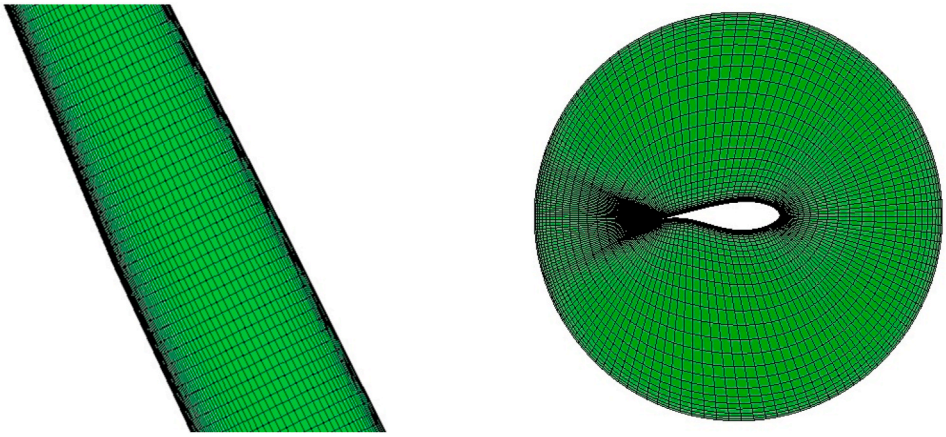

Fig. 8. Mesh on and around the blade geometry.

Table 7
Solver parameter settings used in the flow solver.

Solver		Pressured based
Velocity formulation		Absolute
Time setting		Steady state
Viscous model		k-ω SST
Material		Fluid (air)
Boundary condition	Inlet	Velocity-inlet
	Outlet	Pressure-outlet
	Blade	Stationary wall – no slip
	Vertical surface	Symmetry
Pressure -velocity coupling		SIMPLE
Discretization	Gradient	Least squares cell based
	Pressure	STANDARD
	Momentum	Second order upwind
	Turbulence kinetic energy	First order upwind
	Turbulence dissipation rate	

Table 8
Pitch angle optimisation for higher velocities.

Velocity (m/s)	Original Pitch angle (°)	Reduced pitch angle by °	Optimised pitch angle by °	Optimised pitch angle (°)
12	3.96	1.00	1.00	2.96
16	9.90	1.00, 1.25	1.25	8.65
20	13.91	1.25, 1.35	1.35	12.56
25	18.18	1.25, 1.35, 1.50	1.50	16.68

Table 9
Pitch angle sensitivity study for 16 m/s.

	Pitch angle sensitivity study (CFD)		QBlade results		Error (%)	
Pitch angle (°)	Thrust (MN)	Power (MW)	Thrust (MN)	Power (MW)	Thrust	Power
8.90	1.574	18.123	1.695	20.20	−7.12	−10.28
8.65	1.681	19.554			−0.79	−3.19

Considering maintenance and operational costs due to very large amount of power being generated, any increase in size can be justified (Vartan, 2021). The goal is however to design and manufacture fully functional wind turbines that are also cost effective. When considering an upscaling approach to define the characteristics of an intended large scale offshore wind turbine, similarities are usually assumed with geometry and aerodynamic concepts of wind turbines, at constant tip speed between the baseline and the upscaled design (Yurdusev et al., 2006; Whitcomb, 1976). Through this approach, structural properties and vital operations are established; this also helps determine the technological difficulties when upscaling (Kong et al., 2005).

When similarities with geometry are considered, weight m and power P scaling are usually considered. Table 1 lists the properties of the International Energy Agency (IEA) 5 MW wind turbine considered as the base model here, using a simple scaling approach (Sieros et al., 2012). This includes the hub height, blade diameter and tip speed for 5 up to 20 MW wind turbines.

In the current research, the "DTU 10 MW reference wind turbine" has been upscaled to obtain a 20 MW wind turbine. Classical similarity rules have been applied to establish the final design, and the rotor area has been doubled to obtain twice the amount of power. Assuming similarities in geometry, mass and power can be scaled as:

$$m \sim sf^3 P \sim sf^2 \tag{1}$$

with sf the geometric scaling factor defined as:

$$sf = \sqrt{\frac{Expected\ power\ after\ upscaling}{Power\ of\ existing\ upscalable\ model}} = \sqrt{\frac{20}{10}} \tag{2}$$

3. Methodology

The baseline (Bak et al., 2013) wind turbine blade has been upscaled to achieve 20 MW power using the above-described methodologies. Wind turbine blades with a larger span will produce more energy. Large blades provide a wide area for the airflow to pass across, resulting in higher rotational power and force (Hau, 1981). However, the overall contribution made by increasing the blade span length as compared to other components, makes a real difference. Both the blade size and the velocity of the wind will determine the aerodynamic performance of the blade, this can be achieved using power/energy formulas. At a given swept area of the blade and velocity, the level of energy available in the airflow can be determined as:

$$E = \frac{1}{2}\dot{m}U^2 \tag{3}$$

with $\dot{m}$ the mass flow rate, and U the wind velocity.

Assuming a sea-level wind density of $\rho = 1.23\ kg/m^3$, the mass flow rate can be determined as:

$$\dot{m} = \rho U\ \pi r^2 \tag{4}$$

where $A = \pi r^2$ is the rotor swept area

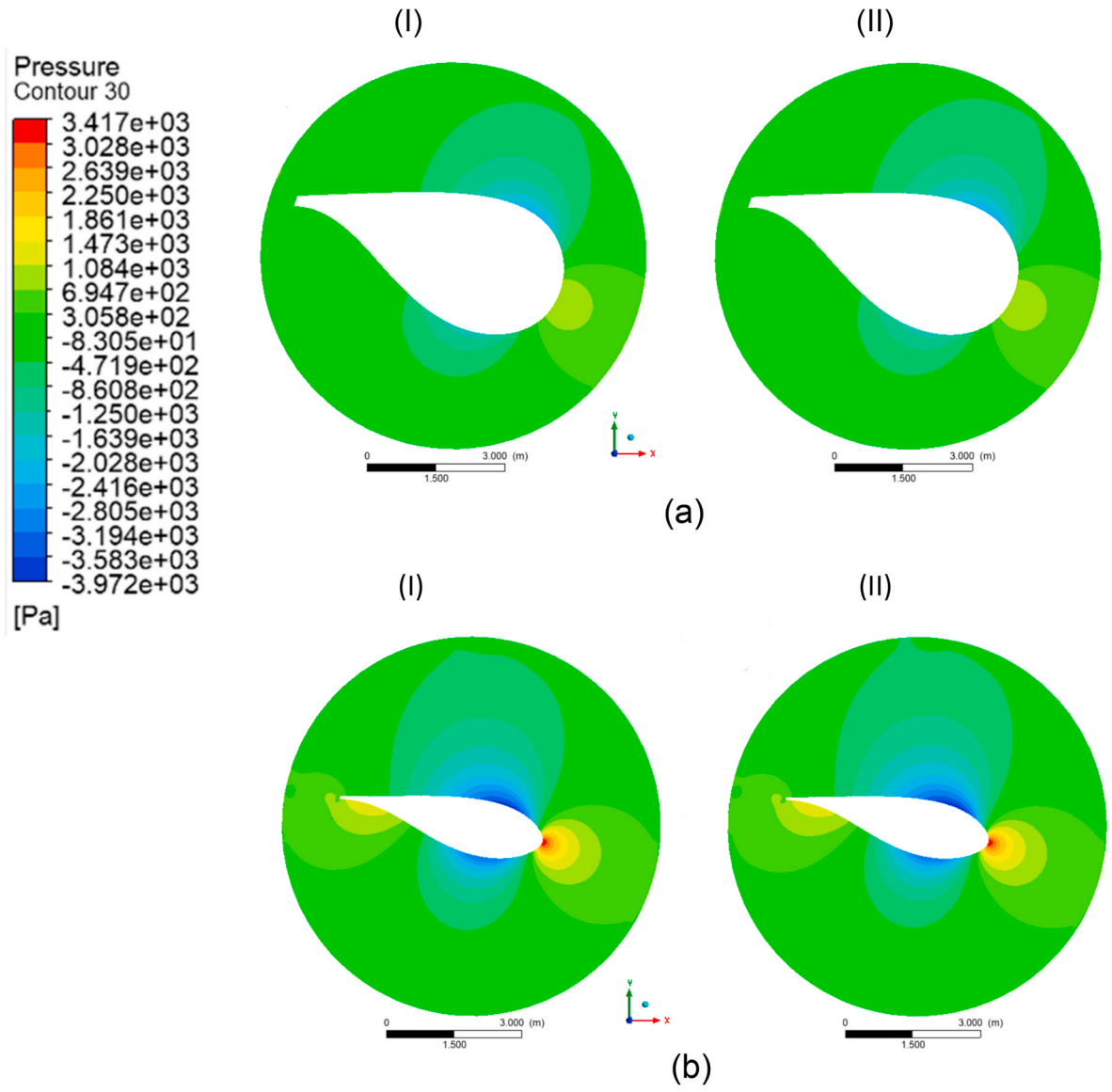

Fig. 9. Pressure contour plots for pitch angle (I) 8.9° and (II) 8.65° at (a) 30% and (b) 60% of the span – 16 m/s.

It appears clearly from Equation (4), that the mass flow rate is directly proportional to the rotor radius squared (r^2). Hence the longer the span the higher the mass flow rate, and therefore the higher the power/energy production (Jonkman et al., 2009). For large blades, a large nacelle is required, which therefore requires a massive tower. Hence, the blade length must be selected carefully to produce maximum power output and remain cost effective.

4. QBlade based results

The "DTU 10 MW RWT" (Bak et al., 2013) wind turbine blade was upscaled to work for a 20 MW offshore wind turbine. Note that in the research presented here, only the aerodynamic design is investigated as it is key-element to improve the power output, even though structural and aero-servo-elastic properties are also important. The upscaled parameters of the 10 and 20 MW turbines are listed in Table 2.

4.1. Upscaled blade geometry

The "DTU 10 MW RWT" (Bak et al., 2014) has a relatively light rotor with aerofoils of high thickness, which increase the structural stiffness of the blade. Available aerofoils such as the FFA-W3 series are used here. These series of aerofoils are often selected for modern large-scale offshore wind turbine designs. The relative thickness of FFA aerofoils varies from 21.1 to 36.0%. In the current studies, aerofoils with relative thicknesses of 24.1, 30.1, and 36%, were selected, as shown in Fig. 1. The 48% thick aerofoil was designed by multiplying the coordinates normal to the chord of the 36% thick aerofoil by 1.333, i.e. by $\left({}^{48\%}/_{36\%}\right)$, and the 60% thick aerofoil was derived by a smooth interpolation between the cylindrical shape at the blade root, and the 48% thick aerofoil (Bak et al., 2013).

Using the geometrical parameters in Table 3, the 3D blade geometry shown in Fig. 2 has been redesigned in QBlade.

The length of the blade is increased to 122 m with a hub radius of 4 m, and this blade is placed at the centre of the hub, hence the radius of the blade considered is 126 m.

At this stage of the work, the chord and twist of the blade remain identical to that of the baseline model. The optimisation procedure will highlight the effects of extending the blade length.

The maximum $C_P = 0.467$ for the current blade is obtained at a tip speed ratio of 9 and for a pitch angle of 0°, as shown in Fig. 3. As mentioned previously, 100% extraction of energy from the wind is not

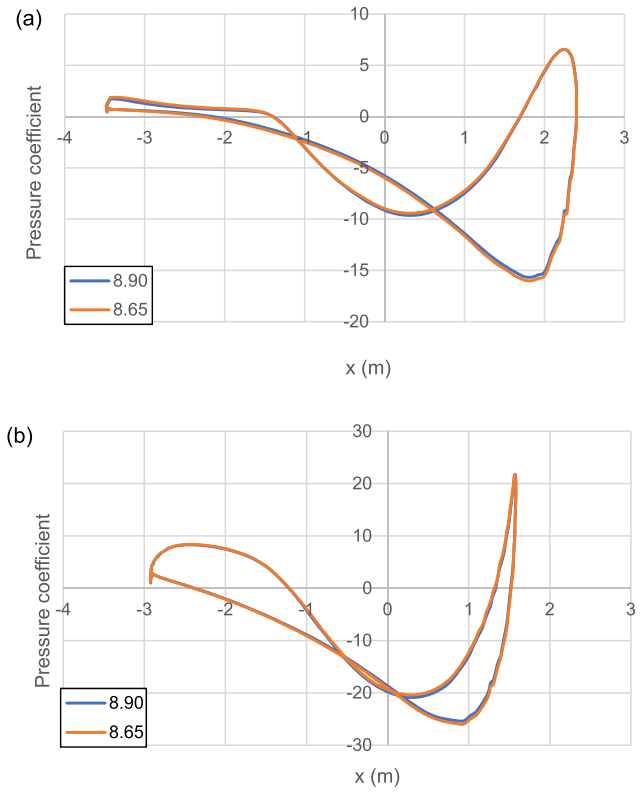

Fig. 10. Pressure coefficient for pitch angles 8.9° and 8.65° at (a) 30% and (b) 60% of the span – 16 m/s.

Table 10
Pitch angle sensitivity study at 25 m/s.

	Pitch angle sensitivity study (CFD)		QBlade results		Percentage of error	
Pitch angle (degree)	Thrust (MN)	Power (MW)	Thrust (MN)	Power (MW)	Thrust	Power
16.93	0.997	16.294	1.24	20.2	−19.62	−19.33
16.83	1.046	17.557			−15.64	−13.08
16.68	1.104	19.023			−10.98	−5.82

possible as energy is extracted by slowing the wind down and removing part of its kinetic energy. As the wind is slowed down, the air behind the blade is slower. If further kinetic energy is extracted, the downstream air will block the next intake of air, which will hit a wall of stalled air (Hansen, 2008).

4.2. Simulation results

The upscaled blade was simulated for different rotational speeds and pitch angles. The simulation parameters used to calculate the power and thrust are $\rho = 1.225$ kg/m^3 and $\mu = 1.784 \bullet 10^{-5}$ kg/m-s. The velocity ranges between 5 and 25 m/s, where the rated power output was achieved at 12 m/s. Velocities selected to perform the simulations and to study the flow physics are marked with a '*' symbol in Table 4. These velocities* are selected due to their unique corresponding rotational speed, and to reduce computational resources. Results are then compared with the CFD-based ones obtained with the flow solver ANSYS Fluent.

The rotational speed was varied between 4 and 10 rpm and the optimised rotational speed was selected at a 0° fixed pitch angle. However, at high wind speeds, between 12 and 25 m/s, this 0° pitch angle did not provide the required power and thrust results, hence, a pitch angle optimisation was carried out. To understand the problem better, for a 0° pitch angle and a velocity of 12 m/s, a 20 MW power was achieved at a rotational speed of 5.4 rpm. This scenario is however not plausible since at a wind speed of 11 m/s, the rotational speed of the blades is 8 rpm, as shown in Table 4. For a wind speed of 12 m/s, blades should therefore rotate at a higher speed, hence higher than 8 rpm.

To achieve the optimum power and thrust results the pitch angle was varied between 0 and 20°. The rotational speed was also varied, and the optimum rotation speed and pitch angle were selected to achieve 20 MW. Table 4 provides the detailed aerodynamic results and the operational parameters, based on QBlade, at different velocities. Fig. 4 shows the aerodynamic performance parameters variation with respect to wind speed.

These aerodynamic results are then compared with those from the "DTU 10 MW RWT" to check both the pattern and agreement. Fig. 5 shows the power and thrust versus velocity. As can be seen, the trends of both the Power and thrust curves for the 20 MW wind turbine obtained with Q-blade agree well with the 10 MW wind turbine blade-based baseline results obtained with the DTU in-house flow solver Ellip-Sys3D. Until the rated velocity of 12 m/s, the power increases linearly and remains constant afterwards until it reaches the cut-out velocity (25 m/s). In the region between the rated and the cut-out velocity, a constant power of 20.2 MW is achieved for the 'new' wind turbine. Henceforth, the ideal power curve is achieved from both the variable rotational speed and the variable pitch angle configuration used in this research.

As shown in Fig. 5, a maximum thrust value of 2.92 MN was achieved for the 'new' design at a wind speed of 11 m/s. At this velocity, the thrust increased from 1.56 MN for the 10 MW turbine to 2.92 MN for the 20 MW turbine, and the corresponding power increased from 11.1 MW to 20.2 MW for a 12 m/s wind velocity. This shows an 87.78% increase in thrust and an 80.83% increase in power with the 'new' design compared to the "DTU 10 MW RWT".

The geometrical design and operational conditions obtained with QBlade are then now considered into the ANSYS CFD software for further comparison of the aerodynamic results.

5. CFD study

This section presents the geometry, mesh generation and flow settings being considered in this work to obtain the CFD results, which are also described in detail.

5.1. Geometry and mesh

The geometrical details described in the previous section are exported from QBlade to build a design model in ICEM CFD. A single blade is selected for the flow simulations, to reduce computational resources, and therefore computational cost and time. One third of the whole geometry is thus considered for the CFD analysis, and the whole computational domain is bounded by periodic boundary conditions, see Fig. 6. A moving refence frame model is applied for this study; hence the blade was placed inside two domains (main and sub-domain) in-order to create the moving reference frame mode, and the fluid interface was connected.

Two different shaped domains were created to understand the domain sensitivity and to establish the most appropriate domain size and its influence on the flow. Those domains are shown in Fig. 6. Regardless of the turbulence model, the size of the domain must be large enough to minimize the interference caused by boundaries. This interference will affect the aerodynamic forces of the wind turbine blade. The distance between the inlet and the blade must also be long enough to ensure that the flow is developed when reaching the blade. It is however important to keep in mind that any unnecessary increase of the domain size will adversely affect the computational cost. Henceforth the domain

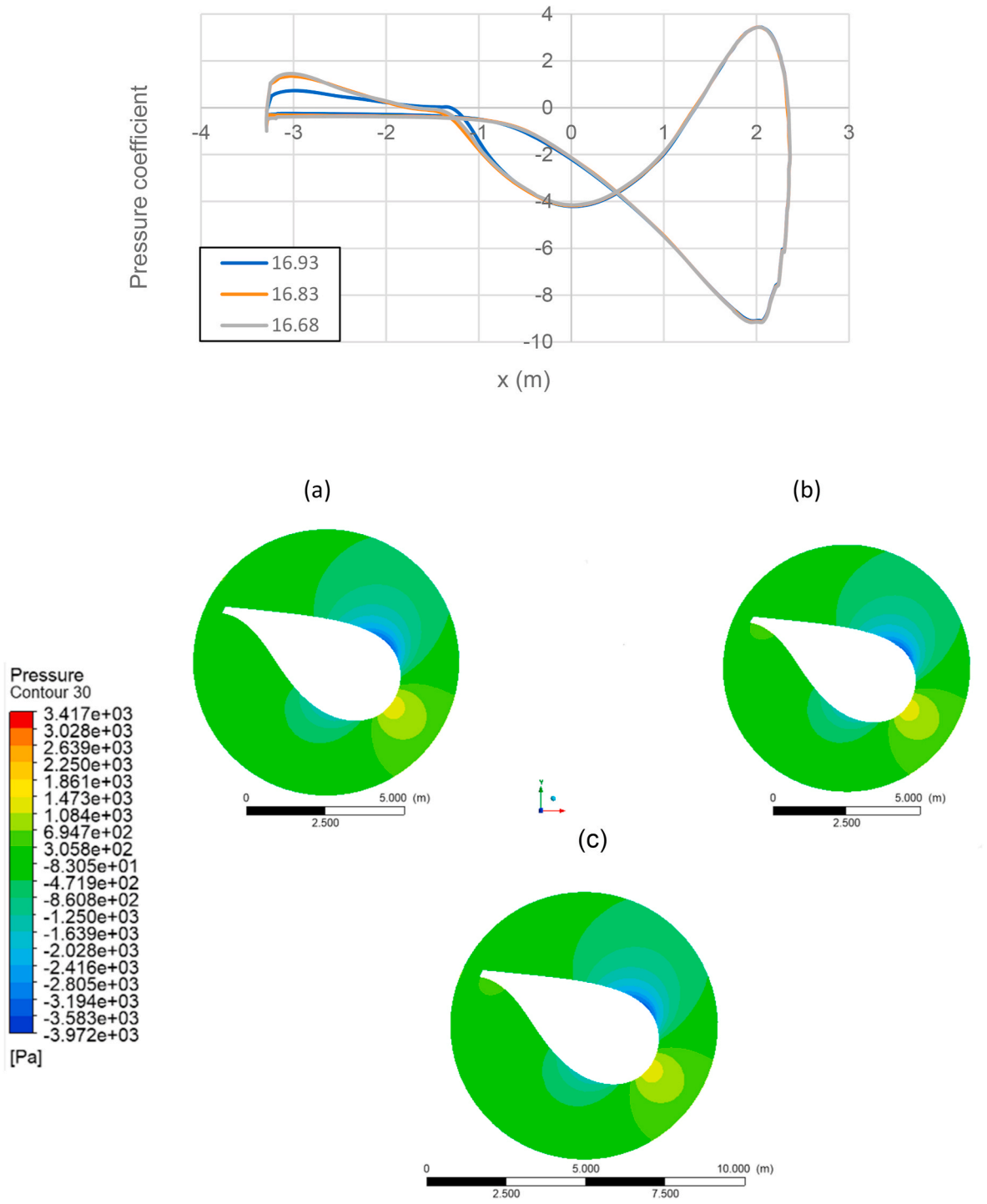

Fig. 11. At velocity 25 m/s pressure coefficient C_P and pressure contour plots for 25 m/s at different pitch angle (a) 16.93° (b) 16.83° (c) 16.68° at 30 % blade span.

size (computational cost) and accuracy of the results (aerodynamic force) are dependent on the grid size and number of cells. Fig. 6 also shows the boundary conditions considered in this study: velocity inlet, pressure outlet, symmetry and as mentioned previously, periodic conditions. Finally, the blade is considered as a wall-type boundary condition.

Fig. 7 shows the side and front view of the domain and provides the corresponding dimensions. The cylindrical domain was selected based on the results obtained and the flow physics near the outlet of the domain. Table 5 provides the dimensions used to determine the effective size of the domain and the turbulence models tested numerically to obtain cost-effective accurate results.

Several turbulence models along with steady/transient models were studied initially for 25 m/s on the 10 MW turbine; the results are summarised in Table 6. The k-ω SST model shows a significant improvement under steady state conditions, when compared with those from DTU and when compared with the other turbulence models tested. This model has also been used successfully in other wind-based studies, see (García Auyanet et al., 2022, 2022b; Bel Laveda et al., 2023) for instance. As can be seen, the error is lower than 1% with this turbulence model while the error obtained with the other models range between 27% and 94%.

Direct numerical simulation (DNS) or large eddy simulation (LES)

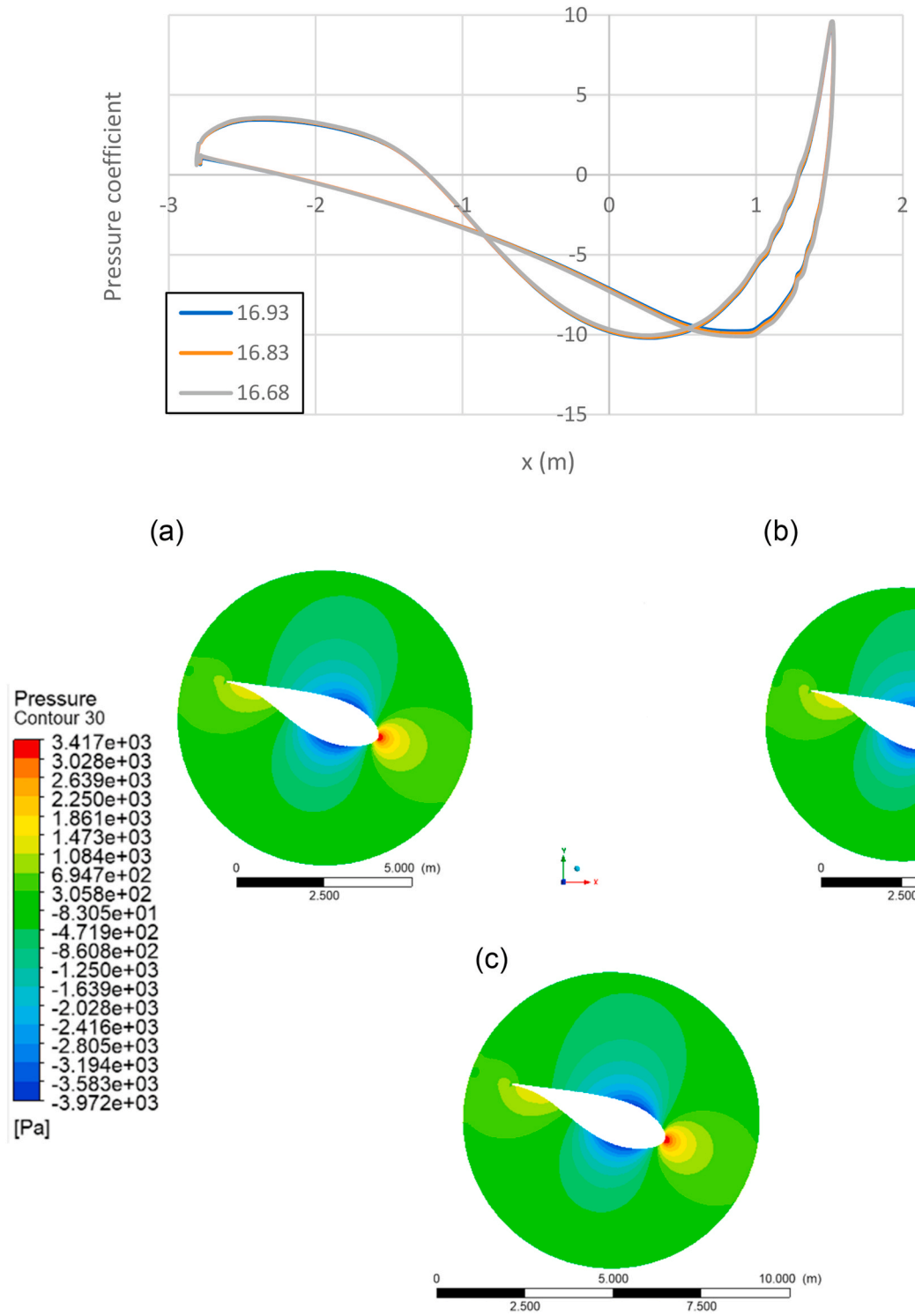

Fig. 12. At velocity 25 m/s pressure coefficient C_P and pressure contour plots for 25 m/s at different pitch angle (a) 16.93° (b) 16.83° (c) 16.68° at 60 % blade span.

would have provided more accurate results. However, those approaches require high computational cost, which make them difficult to use for a high number of simulations.

A hexa O-grid mesh was generated around the blade and in the domain. The outer domain size built for this case was 3D long upstream, 15D long downstream, and 4D long for the outer domain, with D = 252 m, the diameter of the blade. The inner domain was 1.5R long, with R the radius of the rotor. The mesh generated on a section of the blade in the span direction, and around cross section of the blade (aerofoil), is shown in Fig. 8.

The mesh was imported in the flow solver ANSYS FLUENT. The pressure-based solver and the density-based solver are the two types of solvers available in FLUENT. For both solvers, the governing flow equations are discretized using a finite-volume approach. The Equation of State in the density-based solver will determine the pressure field. The pressured-based solver, however, will determine the pressure field by resolving a pressure or a pressure correction equation. This pressure field is obtained by adjusting the continuity and momentum equations

Table 11
Aerodynamic results from CFD for length optimisation.

Velocity (m/s)	Rotational speed (RPM)	Pitch angle (°)	Thrust (MN)	C_t	Power (MW)	C_P
5	4.4	0.00	0.653	0.855	1.50	0.39
6	5.0	0.00	0.908	0.825	2.74	0.42
8	5.4	0.00	1.376	0.704	6.85	0.44
9	6.4	0.00	1.829	0.739	9.91	0.45
10	7.0	0.00	2.235	0.732	13.65	0.45
11	8.0	0.00	2.798	0.757	18.30	0.45
12	9.2	2.96	2.528	0.575	19.36	0.37
16	9.2	8.65	1.681	0.215	19.55	0.16
20	9.2	12.56	1.343	0.110	19.42	0.08
25	9.2	16.68	1.104	0.058	19.02	0.04

which must satisfy the continuity equation by correcting the pressure equation of the velocity field. The governing equations of both algorithms are non-linear and coupled. Energy, continuity, and momentum equations are solved by the density-based solver, this is not the case for the pressure-based approach.

In the present simulation, the pressure-based solver was used to calculate the pressure field since an incompressible flow is considered. The blades operate at a high Reynolds number and the flow is turbulent. The calculated Mach number from the highest tip speed is less than 0.3, which makes the assumption of flow incompressibility valid for this study.

Pressure and velocity are stored at cell centres in FLUENT's co-located approach. The STANDARD pressure interpolation technique was used to acquire the pressure values at the faces. The STANDARD scheme uses momentum equation coefficients to interpolate the pressure values at the faces. The SIMPLE approach, which is the solver's default methodology and is an iterative solution method, was used to obtain the pressure adjustment equation. Table 7 shows the solver parameter settings used in this work. A convergence criterion of 10^{-4} was set for all equations. Coefficients of thrust and torque were monitored to ensure a full convergence of the flow solution.

5.2. Numerical results

The optimised rotational speed was taken from QBlade, and no variation was made in FLUENT. However, the pitch angle was reduced to achieve the rated power output. Table 8 shows the pitch angle reduction carried out to achieve the 20 MW rated power; this pitch angle was reduced for the highest velocities, between 12 m/s and 25 m/s. For the length optimisation case study, the pitch angle for the lowest velocities was zero and the results agreed well with those obtained with QBlade. However, because of the sensitivity observed on the pitch angle, the velocity results with a pitched blade did not agree with QBlade.

The first simulation was carried out for the reduced pitch angle itself. From the baseline study, it was concluded that the minimum reduction in pitch angle required for operating at 12 m/s, was 1°. Hence, for higher velocities, the pitch angle reduction was simulated progressively from the previously optimised pitch angle reduction degree. For instance, in the baseline study at 20 m/s, the optimised pitch angle reduction was of 1.25°, hence the first simulation of the length optimisation was carried out from a 1.25° reduction.

Table 9 shows the aerodynamic results at 16 m/s for different pitch angles. The optimised pitch angle at this velocity is 8.65° with a reduction of 1.25°, showing errors of −0.79% and −3.19% against QBlade-based thrust and power results, respectively. Those low errors are acceptable at this stage of the study because further improvement of the results will be carried out in the next design variants i.e., chord and twist optimisation.

The pressure contour plots and pressure coefficient C_P plots are shown in Figs. 9 and 10, respectively. These plots have been taken at 30 and 60% of the blade span for both pitch angles at a velocity of 16 m/s. As can be seen, there is not much difference between the pitch angle reduction in terms of contour plots, but the slight difference seen for C_P produces an error between 6 and 7% with respect to thrust and power.

Table 10 provides the detailed aerodynamic results obtained from the pitch angle reduction for a wind velocity of 25 m/s. From the optimised pitch angle i.e., 16.68° (1.5° reduction), the errors for thrust and power are −10.98% and −5.82%, respectively. It can thus be established that the required thrust and power are not obtained yet. These results can however be improved further by carrying out a chord and twist

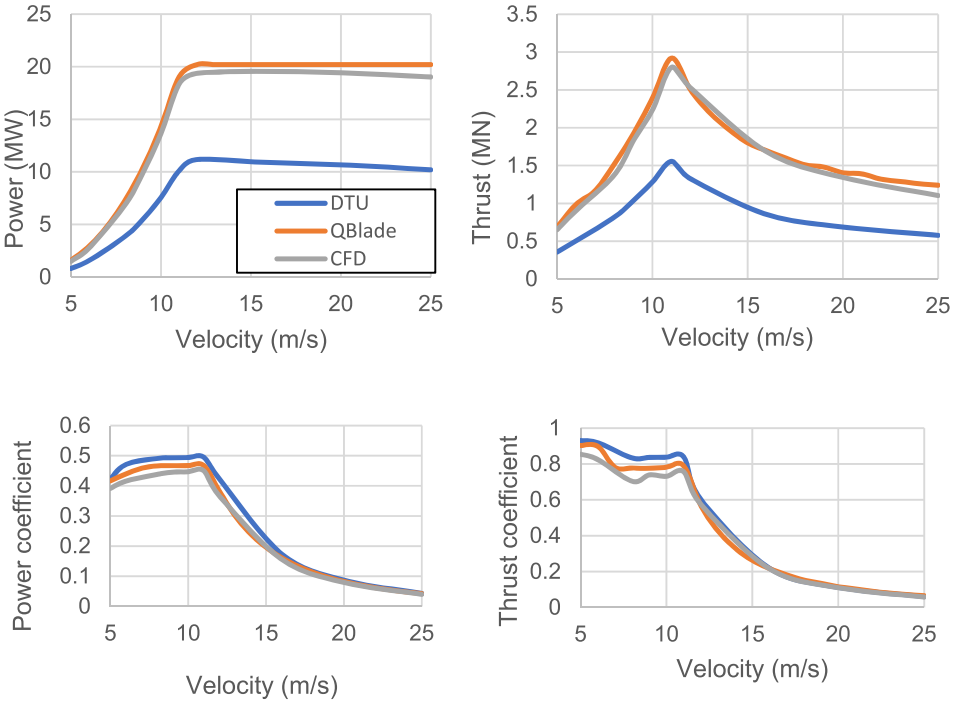

Fig. 13. Aerodynamic results comparison between baseline ("DTU 10 MW RWT"), QBlade, and CFD.

optimisation procedure, this will be the next step of the study.

Figs. 11 and 12 show the pressure contour plots and pressure coefficient C_P at 25 m/s for different pitch angles. Similarly, to the 16 m/s case, the results are established at 30 and 60% of the blade span. The thrust and power were increased by 8.64% and 13.51% compared to the pitch angles of 16.93° and 16.68°, respectively.

The results of the CFD-based length optimisation are shown in Table 11. Similarly, to QBlade, CFD-based results follow the ideal power and thrust curves. A maximum power of 19.55 MW is achieved at 16 m/s whereas a maximum thrust of 2.79 MN is obtained at 11 m/s. In the power curve, the rated power is achieved from the 12 m/s rated velocity to the 25 m/s cut-out velocity.

5.3. Discussion

In the current case, the span of the blade was upscaled from 89.166 m to 126 m to increase the power of the turbine from 10 MW to 20 MW. The geometry of the blade was designed in QBlade to obtain a 20 MW power output with variable rotational speed and variable pitch angle. The optimised power and thrust results were then compared with the baseline results (DTU 10 MW RWT). The power was increased by 80.84% and the thrust by 88.67% at a rated velocity of 12 m/s. From these comparisons it could be concluded that the blade geometry parameters and aerodynamic performance parameters were suitable for further CFD investigations.

The blade geometry was then exported and meshed in ICEM CFD, and flow simulations carried out in the flow solver ANSYS FLUENT. Results at high velocity with a pitch angle did not agree well with the QBlade results due to the flow sensitivity. Hence the pitch angle of the highest velocities, between 12 and 25 m/s was reduced to obtain the required results. This optimisation process increased the power by 73.32% and the thrust by 90.79% when compared to the baseline study.

The comparison between QBlade and CFD-based results showed maximum errors of −10.98 % and −6.05% on the power and thrust coefficients, respectively. It could therefore be concluded that the CFD simulations underpredicted the results when compared to QBlade. The above-mentioned differences were due to the turbulence model considered in the CFD approach, and due to viscosity effects. QBlade does not consider viscous terms, which is a simplification, and the software is based on BEM, whereas CFD solves the Reynolds-Averaged Navier–Stokes equations (RANS), here for the k-ω SST turbulence model. It was thus expected that CFD-based results would be more accurate than QBlade-based results, especially when viscous effects are important.

Fig. 13 shows the comparison between the baseline, QBlade, and CFD-based results. The pattern of the results matches well with each other and the results of QBlade and CFD agree well with each other.

6. Conclusions

The baseline model was studied for boundary condition (BC) interactions and BC placement sensitivity. A cylindrical domain with one blade only forms a more efficient model, due to a significant gain in simulation time and resources when compared to the whole 3-bladed model. Simulations for an inlet boundary placed 3D and 6D upstream of the wind turbine were carried out, and the 3D upstream case showed satisfactory results. This model was thus been selected to reduce further computing time and resources. The outlet was tested at 7D, 10D, 15D, and 20D downstream positions from the turbine. Results, flow interactions, and turbulence intensity worked well when considering the outlet located 15D far from the turbine. The top surface of the domain was set as a symmetry condition (4D high). A rotating cylindrical subdomain was designed at a radius of 1.5R (radius) around the blade. Pressure based steady-state and transient simulations were carried out with different viscous models including Spalart-Allmaras (SA), k-epsilon (standard and realizable), k-omega SST, transition k-kl-omega, and DES. The k-omega SST turbulence model was finally selected for the research due to its higher performance compared to other models. The rotor blade was rotated to a given pitch angle at high velocity, between 12 m/s and 25 m/s. A pitch angle sensitivity study was carried out to obtain accurate results, which were then compared against QBlade and the DTU in-house HAWCStab2 based results. Using similarity rules, the blade length was modified to achieve a power of 20 MW. The new design was meshed, and numerical simulations were carried out under design and off-design conditions. As the blade length was increased, the rotational speed and pitch angle of the blade were also changed. Hence, simulations were carried out for different rotational speeds and pitch angles, and the optimum rotational speed and pitch angle were selected for further design variants. These results were compared with the baseline results, showing that the power and thrust were increased by 80.84% and 88.67%, respectively, at a rated wind velocity of 12 m/s.

Although promising, this numerical study would require further investigation to conclude on the suitability of the proposed blade geometry and length, especially regarding structural integrity aspects.

CRediT authorship contribution statement

Pavana Koragappa: Conceptualization, Formal analysis, Investigation, Methodology, Software, Writing – original draft, Writing – review & editing. **Patrick G. Verdin:** Conceptualization, Methodology, Project administration, Resources, Supervision, Writing – original draft, Writing – review & editing.

Declaration of competing interest

The authors declare that they have no known competing financial interests or personal relationships that could have appeared to influence the work reported in this paper.

Data availability

Data will be made available on request.

Acknowledgements

The authors acknowledge the financial support from “Prabuddha Overseas Scholarship scheme” by the Social Welfare Department of Government of Karnataka, India” for Pavana Koragappa to carry out her PhD degree at Cranfield University, UK.

References

Ashuri, T., Martins, J.R.R.A., Zaaijer, M.B., van Kuik, G.A.M., van Bussel, G.J.W., 2016. Aeroservoelastic design definition of a 20 MW common research wind turbine model. Wind Energy 19 (11).

Bak, C., Bitsche, R.D., Yde, A., 2014. Light rotor: the 10-MW reference wind turbine light rotor: the 10-MW reference wind turbine. Proceedings of EWEA 2012 - European Wind Energy Conference & Exhibition.

Bak, C., Zahle, F., Bitsche, R., Kim, T., Yde, A., Henriksen, L.C., Hansen, M.H., Blasques, J.P.A., Gaunaa, M., Natarajan, A., 2013. The DTU 10 MW Reference Wind Turbine. DTU Wind Energy.

Barlas, T.K., van Kuik, G.A.M., 2010. Review of state of the art in smart rotor control research for wind turbines. Prog. Aero. Sci. 46 (1), 1–27. https://doi.org/10.1016/j.paerosci.2009.08.002.

Bel Laveda, O., Roche, M.A., Phadtare, M., Sauge, L., Xavier, K.J., Bhat, G., Saxena, D., Saini, J.S., Verdin, P.G., 2023. Numerical investigation of aerodynamic performance and structural analysis of a 3D J-shaped based small-scale vertical Axis wind. Turbine. Energies 16, 7024. https://doi.org/10.3390/en16207024.

Bjorck, A., 1990. Coordinates and Calculations for the FFA-Wl-Xxx, FFA-W2-Xxx, FFA-W2-Xxx and FFA-W3-Xxx Series of Airfoils for Horizontal Axis Wind Turbines.

Bossanyi, E.A., 2003. Individual blade pitch control for load reduction. Wind Energy 6 (2), 119–128. https://doi.org/10.1002/we.76.

Chaviaropoulos, P.K., 2007. Similarity rules for W/T up-scaling. UpWind Report, WP 1B4.

Eppler, R., 1997. Induced drag and winglets. Aero. Sci. Technol. 1 (1), 3–15. https://doi.org/10.1016/S1270-9638(97)90019-5.

Farhan, A., Hassanpour, A., Burns, A., Motlagh, Y.G., 2019. Numerical study of effect of winglet planform and airfoil on a horizontal Axis wind turbine performance. Renew. Energy 131, 1255–1273. https://doi.org/10.1016/j.renene.2018.08.017.
Frøyd, L., Dahlhaug, O.G., 2011. Rotor design for a 10 MW offshore wind turbine. Proc. Int. Offshore Polar Eng. Conf. 8, 327–334.
Fuglsang, P., Bak, C., 2004. Development of the risø wind turbine Airfoils. Wind Energy 7 (2), 145–162. https://doi.org/10.1002/we.117.
García Auyanet, A., Santoso, R.E., Mohan, H., Rathore, S.S., Chakraborty, D., Verdin, P. G., 2022. CFD-based J-shaped blade design improvement for vertical Axis wind turbines. Sustainability 14, 15343. https://doi.org/10.3390/su142215343.
García Auyanet, A., Verdin, P.G., 2022. Numerical study of the effect of flap geometry in a multi-slot ducted wind turbine. Sustainability 14, 12032. https://doi.org/10.3390/su141912032.
Gasch, R., Twele, J., 2012. Wind Power Plants: Fundamentals, Design, Construction and Operation, Second. Springer.
Gaunaa, M., Johansen, J., 2007a. Determination of the maximum aerodynamic efficiency of wind turbine rotors with winglets determination of the maximum aerodynamic efficiency of wind turbine rotors with winglets. J Phys Conf Ser. https://doi.org/10.1088/1742-6596/75/1/012006.
Gaunaa, M., Johansen, J., 2007b. Determination of the maximum aerodynamic efficiency of wind turbine rotors with winglets. J Phys Conf Ser 75 (1). https://doi.org/10.1088/1742-6596/75/1/012006.
Hand, S.M.L.M.M., Simms, D.A., Fingersh, L.J., Jager, D.W., Cotrell, J.R., Schreck, S., 2001. Unsteady Aerodynamics Experiment Phase VI: Wind Tunnel Test Configurations and Available Data Campaigns.
Hansen, M.O.L., 2008. Aerodynamics of Wind Turbines, Third. Routledge, London.
Hau, E., 1981. Wind turbines - fundamentals, technologies, application. Economics. https://doi.org/10.4324/9780203103289-9.
Jonkman, J., Butterfield, S., Musial, W., Scott, G., 2009. Definition of a 5-MW Reference Wind Turbine for Offshore System Development. NREL Technical report NREL/TP-500-38060.
Kong, C., Bang, J., Sugiyama, Y., 2005. Structural investigation of composite wind turbine blade considering various load cases and fatigue life. Energy 30, 2101–2114. https://doi.org/10.1016/j.energy.2004.08.016.
Manwell, J.F., McGowan, J.G., Rogers, A.L., 2010. Wind energy explained: theory. Design and Application. https://doi.org/10.1002/9781119994367.
Maughmer, M.D., 2003. Design of winglets for high-performance sailplanes. J. Aircraft 40 (6), 1099–1106. https://doi.org/10.2514/1.10817.
Mourad, M.G., Shahin, I., Ayad, S.S., Abdellatif, O.E., Mekhail, T.A., 2020. Effect of winglet geometry on horizontal Axis wind turbine performance. Engineering Reports 2 (1), 1–19. https://doi.org/10.1002/eng2.12101.
Peeringa, J., Brood, R., Ceyhan, O., Engels, W., de Winkel, G., 2011. Upwind 20 MW wind turbine pre-design. In: Technical Report Tech. Rep. ECN, Paper No. ECN-E–11-017. Energy research Centre of the Netherlands, Peten, the Netherlands.
Schepers, J.G., Schreck, S.J., 2019. Aerodynamic measurements on wind turbines. Wiley: WIREs Energy and Environment 8 (1), 1–25. https://doi.org/10.1002/wene.320.
Shimizu, Y., Kamada, Y., 2001. Studies on a horizontal Axis wind turbine with passive pitch-flap mechanism (performance and flow analysis around wind turbine). Journal of Fluids Engineering, Transactions of the ASME 123 (3), 516–522. https://doi.org/10.1115/1.1375817.
Sieros, G., Chaviaropoulos, P., Sørensen, J.D., Bulder, B.H., Jamieson, P., 2012. Upscaling wind turbines: theoretical and practical aspects and their impact on the cost of energy. Wind Energy 15 (1), 3–17. https://doi.org/10.1002/we.527.
Sørensen, J.N., 2011. Aerodynamic aspects of wind energy conversion. Annu. Rev. Fluid Mech. 43, 427–448. https://doi.org/10.1146/annurev-fluid-122109-160801.
Thé, J., Yu, H., 2017. A critical review on the simulations of wind turbine aerodynamics focusing on hybrid RANS-LES methods. Energy 138, 257–289. https://doi.org/10.1016/j.energy.2017.07.028. Available at:
Van Langen, P., Hendrinks, B., 2010. 5 MW UpWind reference wind turbine data. In: Technical Report Tech. Rep. UpWind Internal Report. Energy research Centre of the Netherlands, Peten, the Netherlands.
Vartan, Starre, 2021. What Is Wind Energy? Definition and How it Works. Treehugger. https://www.treehugger.com/what-is-wind-energy-5097217.
Versteeg, H.K., Malalasekera, W., 2012. Introduction to computational fluid Dynamics. Introductory Fluid Mechanics 343–416. https://doi.org/10.1017/cbo9780511761348.011. Available at:
Whitcomb, R.T., 1976. A design approach and selected wind tunnel results at high subsonic speeds for wing-tip mounted winglets. Nasa Tn D-8260 1–33. https://ntrs.nasa.gov/archive/nasa/casi.ntrs.nasa.gov/19760019075.pdf.
Wilson, A.B., 2020. Offshore Wind Energy in Europe, pp. 1–6. https://www.europarl.europa.eu/RegData/etudes/BRIE/2020/659313/EPRS_BRI(2020)659313_EN.pdf.
Wilson, R.E., S, L.P.B., 1974. Applied Aerodynamics of Wind Power Machines.
Yurdusev, M.A., Ata, R., Çetin, N.S., 2006. Assessment of optimum tip speed ratio in wind turbines using artificial neural networks. Energy 31 (12), 2153–2161. https://doi.org/10.1016/j.energy.2005.09.007.